Zhang *et al. Complex Eng Syst* 2024;4:18
DOI: 10.20517/ces.2024.55

Complex Engineering Systems

Research Article

Open Access

Path loss prediction for air-to-ground communication links via scenario transfer technology

Guanjie Zhang[1], Taiya Lei[2], Xiaofeng Huo[3], Yanbin Li[1], Mengjie Geng[1], Hongjie Yang[1], Yuxin Yang[2], Xiaomin Chen[2]

[1]The 54th Research Institute of China Electronics Technology Group Corporation, Shijiazhuang 050081, Hebei, China.
[2]Nanjing University of Aeronautics and Astronautics, Nanjing 211106, Jiangsu, China.
[3]Qingdao Metro Group Co., Ltd, Qingdao 266000, Shandong, China.

Correspondence to: Dr. Xiaomin Chen, Nanjing University of Aeronautics and Astronautics, Nanjing 211106, Jiangsu, China. E-mail: chenxm402@nuaa.edu.cn

How to cite this article: Zhang G, Lei T,Huo X, Li Y, Geng M, Yang H, Yang Y, Chen X. Path loss prediction for air-to-ground communication links via scenario transfer technology. *Complex Eng Syst* 2024;4:18. http://dx.doi.org/10.20517/ces.2024.55

Received: 29 Aug 2024 **First Decision:** 21 Sep 2024 **Revised:** 26 Sep 2024 **Accepted:** 27 Sep 2024 **Published:** 30 Sep 2024

Academic Editor: Hamid Reza Karimi **Copy Editor:** Fangling Lan **Production Editor:** Fangling Lan

Abstract

Path loss (PL) is a significant channel parameter for the link budget in unmanned aerial vehicle-aided communications. This study introduces an innovative neural network model to estimate PL for air-to-ground communication links. Utilizing the geometric characteristics of varied physical environments, the model accurately predicts PL in diverse communication scenarios. A back-propagation neural network technique is introduced for extrapolating PL under both line-of-sight and non-line-of-sight conditions. A dataset acquisition strategy, comprising scenario reconstruction and advanced ray-tracing techniques, is employed to foster the model's training and evaluation. Finally, the proposed model is fully trained in diverse communication scenarios, and then used to predict the PLs in a new communication scenario generated by the International Telecommunication Union standard at 28 GHz. The results demonstrate that the extrapolated PLs of the proposed model are well consistent with the reference results. As existing PL models and standard PL models aim at several specifically defined scenarios, the proposed model can predict the PLs in some undefined and unknown scenarios.

Keywords: A2G communication, unmanned aerial vehicle (UAV), path loss (PL) prediction, back-propagation neural network (BPNN)

1. INTRODUCTION

Unmanned aerial vehicle (UAV) communications have gained attention in both civilian and military fields due to their cost efficiency and versatility[1,2]. Furthermore, UAVs are increasingly being used in the delivery of goods and medical supplies, particularly in remote or inaccessible areas, showcasing their potential to transform logistics and healthcare services[3]. The integration of UAVs into communication networks also opens up new possibilities for enhancing connectivity in areas with limited infrastructure, thereby bridging the digital divide[4]. Recently, millimeter-wave (mmWave) communication has gained popularity due to its significant advantages, such as wide bandwidth, high-speed data transmission, and low latency. The mmWave spectrum offers a vast amount of available bandwidth, which is essential for meeting the growing demand for data-intensive applications[5]. Using mmWave frequencies allows for smaller antennas, which promotes considerable directional gain and enhances spatial reuse. This frequency range is particularly suitable for urban environments where high data rates are required. Moreover, mmWave communication reduces signal interference and increases security and privacy, as its narrow beams are less susceptible to interception compared to traditional frequency bands[6]. The deployment of mmWave technology is also seen as a key enabler for the next generation of wireless networks, including 5G and beyond[7].

Accurate path loss (PL) modeling and prediction are crucial for developing and improving wireless networks. These models are instrumental in determining coverage areas, enabling network designers to ensure that the signal reaches the intended locations effectively[8]. They also play a vital role in evaluating transmission distances, helping to optimize the placement of transmitters (Tx) and receivers (Rx) to maintain robust communication links[9]. Furthermore, understanding PL is essential for measuring signal strength within the network infrastructure, which is critical for maintaining reliable and high-quality service[10]. However, in urban scenarios, establishing low-altitude air-to-ground (A2G) channel models becomes increasingly complex. Urban scenarios include a large number of buildings and trees that typically obstruct the line-of-sight (LoS) paths. This leads to the multipath effect and produces additional signal attenuation. Owing to the complexity of this case, it is impractical and unfeasible to conduct detailed field measurements of each type of scenario[11]. Therefore, it is imperative to develop a robust and effective A2G PL prediction model that can be adapted to different urban scenarios.

1.1 Related works

There are two common methods for modeling PL in wireless communication systems: deterministic modeling methods and empirical modeling methods[12,13]. Deterministic modeling, based on the principles of physics, employs mathematical formulations to delineate the impact of obstacles and environmental variables on signal strength during propagation. Ray tracing (RT) is a well-known method for tracking rays from a Tx to a Rx. It shows how rays are reflected, refracted, and diffracted along their path, and thus calculates the signal attenuation[14]. For example, the authors in[15] proposed a three-dimensional (3D) scattering scene reconstruction method based on digital maps. They performed a RT simulation under a campus scenario at 28 GHz and analyzed the impact of scene reconstruction accuracy on channel parameter characteristics. Authors in[16] introduced a 3D RT technique to enhance the accuracy of propagation predictions and computational efficiency in indoor environments at 28 GHz. Field measurement also belongs to the deterministic modeling methods. The UAV channel measurements are performed in a suburban scenario, and the PL parameters are analyzed in[17]. Authors in[18] conducted a wideband A2G channel measurement campaign for fixed-wing UAVs at altitudes of up to 700 m, investigating channel characteristics such as PL and shadow fading (SF). Besides, the authors in[19] conducted UAV-to-Vehicle (U2V) channel measurements in the S and C bands under various low-altitude UAV and mobile vehicle scenarios to analyze PL characteristics.

Due to the complexity and time-consuming nature of deterministic methods, especially for highly dynamic UAV communication scenarios, empirical modeling has become more popular. This approach involves collecting measurement data for statistical analysis to establish a link between PL and its influencing factors,

thereby constructing a mathematical model. Notable empirical models for specific scenarios have been put forth by various organizations to address both visible and obstructed paths. The 3rd Generation Partnership Project (3GPP) has introduced comprehensive PL models that are widely used in the industry for different environmental conditions[20]. Additionally, the WINNER+ project has developed advanced PL models that provide detailed insights and improved accuracy for various propagation environments, further enhancing the understanding of signal behavior in both LoS and non-line-of-sight (NLoS) conditions[21,22]. The close-in (CI) model derived from the empirical model is applied to fit the measurement data to further obtain the statistical properties of PLs with respect to the communication distances[23,24]. However, the strong dependence of empirical modeling on statistical analysis can sometimes cause errors.

In light of this, PL modeling methods incorporating machine learning (ML) are emerging, which offer higher accuracy, flexibility, and adaptability to complex propagation environments[25]. ML-based models can well explain the complex relationship between the input features and the resultant PL, satisfying the demands of high-variability and nonlinear feature scenarios. These models excel in dynamic environments by using the ability to update and retrain with new data. Some examples of such models include deep neural networks (DNN), regression trees, and support vector machines (SVM). In[26], a model was introduced to forecast PL, incorporating considerations of path delay, the carrier frequency, and reflection angle (RA) concurrently. However, a common challenge these predictive models face is their limited ability to generalize across differing scenarios. Recently, the authors in[11] proposed a method based on neural networks (NNs) for transferring channel parameter scenarios. They initially conducted measurements of the channel properties, including PL, K-factor, and the root mean square delay spread in a semi-urban scenario. Then, the channel characteristics in dense-urban scenario are predicted by this network. Despite its innovation, this method requires RT simulation data from both initial and target scenarios to create a transfer matrix, making the direct link between geometry and channel characteristics complex. Additionally, it involves significant computational effort and complexity.

1.2 Motivation

Deterministic PL prediction models are time-consuming and have high computational complexity when dealing with complex environments. Empirical prediction models rely on a predefined mathematical equation, which may not accurately represent the inner relationship between PL and the other factors for each communication scenario. ML-based PL prediction models do not need an empirical equation, but current networks are usually trained for specific scenarios, which leads to insufficient cross-scenario prediction ability. Thus, to avoid a large amount of fitting and training under different scenarios, it has become necessary to propose an efficient PL prediction method with cross-scenario ability for A2G mmWave communications.

1.3 Contributions

Motivated by the above background and current research gaps, this paper proposes an innovative NN model. The contributions and novelties are summarized as follows:

- This paper proposes a back-propagation NN (BPNN)-based PL prediction model for A2G communication systems. The network includes scenario parameters as inputs for the first time. Combined with horizontal distance and height, the proposed model can accurately predict the PLs in new scenarios using training data from limited scenarios.
- To train the NN model, the data acquisition method from RT simulations is introduced. The reconstruction of statistical scenarios simplifies the reconstruction process, and reduces cost and complexity. Appropriate transceiver layouts enable the model to improve its ability to predict PL under various scenarios accurately.
- The proposed model is validated and analyzed in an urban scenario at 28 GHz. Simulations and analysis show that all factors, i.e., scenario characteristics, horizontal distance and altitude, have a significant impact on PL. Furthermore, comparison with the PL results of 3GPP standards shows that our method achieves higher accuracy. This result establishes a new standard for accurate PL prediction models in UAV

communication.

The rest of the paper is organized as follows. In Section 2, a cross-scenario PL prediction model based on ML is given. Section 3 gives the details of the training model and methods of data acquisition. The simulation and validation of the proposed method are given in Section 4. Section 5 draws the conclusions.

2. NEURAL NETWORK-BASED PL PREDICTION MODEL

The empirical PL models are usually described by parameterized expressions. The free space PL (FSPL) is the basic method for describing PLs in the obstacle-free environment. However, the model does not consider practical considerations such as reflections, diffraction, and scattering. Thus, it is less accurate in complex environments. Wireless signal propagation is closely linked to complex environments such as areas with buildings and other obstructions[27]. The 3GPP PL model is suitable for these scenarios: urban, suburban, rural, and indoor environments. However, it is more complex to implement and requires detailed environmental parameters.

To overcome the limitations of traditional models such as FSPL and 3GPP, ML algorithms have emerged as a promising alternative, capable of learning from large datasets to improve PL predictions in dynamic environments. However, it is very complicated to precisely define the correlation between PL and various scenario types. To address this challenge, we parametrically characterize the physical geometry of scenarios defined by the International Telecommunication Union-Radiocommunication Sector (ITU-R)[28] as input parameters, and a PL prediction model via ML is proposed. In this paper, our focus is not to improve the BPNN technology; rather, we adopt it to solve the cross-scenario problem of PL prediction. In this way, we do not need to acquire data and train the network again in a new scenario, which greatly reduces the complexity of cross-scenario PL prediction. This innovative model is adept at autonomously identifying deep relationships between network input parameters and output data, avoiding the empirical formulation characteristic of stochastic methods. Moreover, it outperforms the deterministic approach in terms of time efficiency, especially for massive datasets. The proposed PL model based on BPNN for LoS and NLoS paths can be expressed as

$$P^{\mathrm{LoS/NLoS}} = f_{\mathrm{BPNN}}^{\mathrm{LoS/NLoS}}\left(\alpha, \beta, \gamma, h^{\mathrm{LoS/NLoS}}, s^{\mathrm{LoS/NLoS}}; \mathbf{w}, \mathbf{b}, \boldsymbol{\sigma}\right) \tag{1}$$

where $f_{BPNN}(\cdot)$ represents the mapping function of the BPNN, which is shaped by the network's architecture, while $\mathbf{w}$, $\mathbf{b}$ and $\boldsymbol{\sigma}$ signify the network's weight matrix, bias matrix, and activation function matrix, respectively. h indicates the height of the Tx above ground and s denotes the horizontal separation between the Tx and the Rx α, β and γ correspond to the ratio of land area covered by buildings to total land area, the mean number of buildings per unit area(buildings/ km^2), and a factor that influences the distribution of building heights, respectively. The Rayleigh probability distribution, denoted as $P(H)$, is related with the parameter γ:

$$P(H) = \frac{H}{\gamma^2} \exp\left(\frac{-H^2}{2\gamma^2}\right) \tag{2}$$

The model is designed to capture the complex relationships between the input features and the PL. Trained based on the dataset from various scenarios and different distances, the network can predict the PL accurately according to a new group of inputs. The parameters $\mathbf{w}$, $\mathbf{b}$ are optimized during the training process to minimize the difference between the predicted and actual PL values. $\boldsymbol{\sigma}$ is crucial for introducing non-linearity into the model. Without non-linearity, the NN would essentially be a linear regression model, regardless of the number of layers. $f_{BPNN}(\cdot)$ denotes a trained BPNN model that accepts multiple input features and, after layers of computation (including linear transformation and nonlinear activation), finally outputs the predicted value of PLs. In this paper, we introduce a NN designed to facilitate a five-input (α, β, γ, h, s) to single-output P.

3. PL PREDICTION FOR THE CROSS-SCENARIO

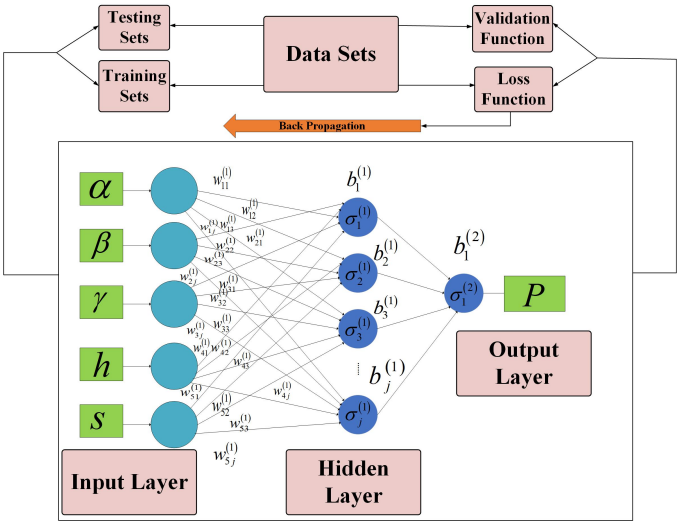

Figure 1. BPNN-based framework of path loss prediction.

3.1 BPNN-based PL prediction

Under the LoS conditions, the PL is predominantly influenced by the distance between the Tx and Rx, given the absence of obstructions along their direct path. The input variables, namely the height h and the horizontal distance s, play a crucial role in determining the P. Consequently, it becomes unnecessary to incorporate an extensive array of scenario parameters such as α, β and γ. By focusing on h and s, we aim to clarify the impact of altitude and horizontal distance on P, and a detailed examination of these parameters is presented in Section 4.

Under NLoS conditions, PL is influenced by either reflection or diffraction phenomena. It is observed that propagation paths of identical distances between the Tx and Rx can exhibit markedly different PL values. This variation underscores the necessity of incorporating a broader range of scenario parameters into the input dataset to enhance the model's capability to discern the intricate relationship between input variables and the resulting PL. The framework for PL prediction utilizing a BPNN for both LoS and NLoS paths is illustrated in Figure 1. Central to the BPNN architecture is the arrangement of an input layer, hidden layers, and an output layer. As depicted in Figure 1, the input layer is designed with five neurons, while the output layer features a single neuron. The original data sets denote $\{P_{all}^{\mathrm{LoS/NLoS}}, \alpha_{all}^{\mathrm{LoS/NLoS}}, \beta_{all}^{\mathrm{LoS/NLoS}}, \gamma_{all}^{\mathrm{LoS/NLoS}}, h_{all}^{\mathrm{LoS/NLoS}}, s_{all}^{\mathrm{LoS/NLoS}}\}$ All of them can be obtained by the data acquisition in Section 3. Then, these data sets are divided into two parts by the proportion of 8:2 randomly, i.e., training set $\{P_{tr}^{\mathrm{LoS/NLoS}}, \alpha_{tr}^{\mathrm{LoS/NLoS}}, \beta_{tr}^{\mathrm{LoS/NLoS}}, \gamma_{tr}^{\mathrm{LoS/NLoS}}, h_{tr}^{\mathrm{LoS/NLoS}}, s_{tr}^{\mathrm{LoS/NLoS}}\}$, and testing set, $\{P_{test}^{\mathrm{LoS/NLoS}}, \alpha_{test}^{\mathrm{LoS/NLoS}}, \beta_{test}^{\mathrm{LoS/NLoS}}, \gamma_{test}^{\mathrm{LoS/NLoS}}, h_{test}^{\mathrm{LoS/NLoS}}, s_{test}^{\mathrm{LoS/NLoS}}\}$, respectively. The data from the training set are used to train the model. The output prediction value of PL can be expressed as

$$P_{trpre}^{\mathrm{LoS/NLoS}} = \sigma\left(\mathbf{w}^{\mathrm{T}}\mathbf{x} + \mathbf{b}\right) \tag{3}$$

where $\mathbf{x}$ represents the input matrix of training set $\{\alpha_{tr}^{\mathrm{LoS/NLoS}}, \beta_{tr}^{\mathrm{LoS/NLoS}}, \gamma_{tr}^{\mathrm{LoS/NLoS}}, h_{tr}^{\mathrm{LoS/NLoS}}, s_{tr}^{\mathrm{LoS/NLoS}}\}$. In this paper, the Tansig function is employed from the input layer to the hidden layer to enhance the network's nonlinear prediction capabilities. For the transition from the hidden layer to the output layer, the Purelin function is applied. These functions are expressed as

$$\sigma_{\mathrm{tansig}}(x) = \frac{2}{1 + e^{-2x}} - 1 \tag{4}$$

$$\sigma_{\mathrm{purelin}}(x) = x \tag{5}$$

At the beginning of the training phase, the weight and bias parameters of each neuron in the network have not yet been optimized, resulting in significant differences between the predicted and reference values. To overcome this difference, it is crucial to establish a suitable loss function. This function helps to continuously refine the neuron parameters through back-propagation, thus minimizing the errors. The loss function utilized in this paper is expressed as

$$L\left(\mathbf{w},\mathbf{b},\sigma\right)=\frac{1}{2R}\sum_{r=1}^{R}\left(P_{trpre,r}^{\mathrm{LoS/NLoS}}-P_{tr,r}^{\mathrm{LoS/NLoS}}\right)^{2} \tag{6}$$

where R is the sum of training set, $P_{tr,r}^{\mathrm{LoS/NLoS}}\in P_{tr}^{\mathrm{LoS/NLoS}}$ and $P_{trpre,r}^{\mathrm{LoS/NLoS}}\in P_{trpre}^{\mathrm{LoS/NLoS}}$. Following the principles of stochastic gradient descent (SGD), the back-propagation algorithm is employed to iteratively adjust the weight and bias matrices, as detailed below

$$w_{ij}^{(k)}=w_{ij}^{(k)}-l\frac{\partial L(\mathbf{w},\mathbf{b},\sigma)}{\partial w_{ij}^{(k)}}+m\Delta w_{ij}^{(k)} \tag{7}$$

$$b_{j}^{(k)}=b_{j}^{(k)}-l\frac{\partial L(\mathbf{w},\mathbf{b},\sigma)}{\partial b_{j}^{(k)}}+m\Delta b_{j}^{(k)} \tag{8}$$

where $\partial(.)$ represents the partial derivatives, $w_{ij}^{(k)}\in\mathbf{w}$ and $b_{ij}^{(k)}\in\mathbf{b}$ are the connection weight values and bias value of the j th neuron in the k th layer of the network and the i th neuron in the previous layer, respectively. l is the learning rate of the NN and m is the momentum factor. the output prediction value of PL from testing dataset can be expressed as

$$P_{testpre}^{\mathrm{LoS/NLoS}}=f_{\mathrm{BPNN}}^{\mathrm{LoS/NLoS}}\left(\alpha_{testpre}^{\mathrm{LoS/NLoS}},\beta_{testpre}^{\mathrm{LoS/NLoS}},\gamma_{testpre}^{\mathrm{LoS/NLoS}},h_{testpre}^{\mathrm{LoS/NLoS}},s_{testpre}^{\mathrm{LoS/NLoS}};\mathbf{w},\mathbf{b},\sigma\right) \tag{9}$$

Root mean square error (RMSE) is proposed as the validation function to evaluate the performance of NN using the testing dataset[29], which can be expressed as

$$RMSE=\sqrt{\frac{1}{T}\sum_{t=1}^{T}\left(P_{testpre,t}^{\mathrm{LoS/NLoS}}-P_{test,t}^{\mathrm{LoS/NLoS}}\right)^{2}} \tag{10}$$

where T is the sum of testing set, $P_{test,r}^{\mathrm{LoS/NLoS}}\in P_{test}^{\mathrm{LoS/NLoS}}$ and $P_{testpre,r}^{\mathrm{LoS/NLoS}}\in P_{testpre}^{\mathrm{LoS/NLoS}}$.

Training concludes and the network stabilizes once any of the following criteria are met: the loss function diminishes to a predetermined threshold, the number of training epochs is reached, or the gradient's decrease meets a predefined value. If the performance is appropriate, this network could be saved and a new group of input parameters; i.e., $\alpha_{new},\beta_{new},\gamma_{new},h_{new},s_{new}$ are used to generate the corresponding prediction value of PL.

3.2 RT-based dataset acquisition

In the BPNN PL prediction model, dataset acquisition is crucial for tuning NN parameters and ensuring accuracy. Due to the complexity of developing an mmWave A2G channel sounder, we are unable to acquire enough training data at the mmWave band. Considering that the RT is one of the accurate channel modeling methods, this paper chooses to acquire the dataset via the RT simulation. The dataset acquisition involves 3D scenario reconstruction and RT simulation.

Traditional methods for scenario reconstruction, such as point-cloud and digital mapping technologies, demand detailed scene information, such as the scatter location, size, shape, and material, making the process complex. To overcome this obstacle, the ITU standard organization has introduced a virtual city-based 3D

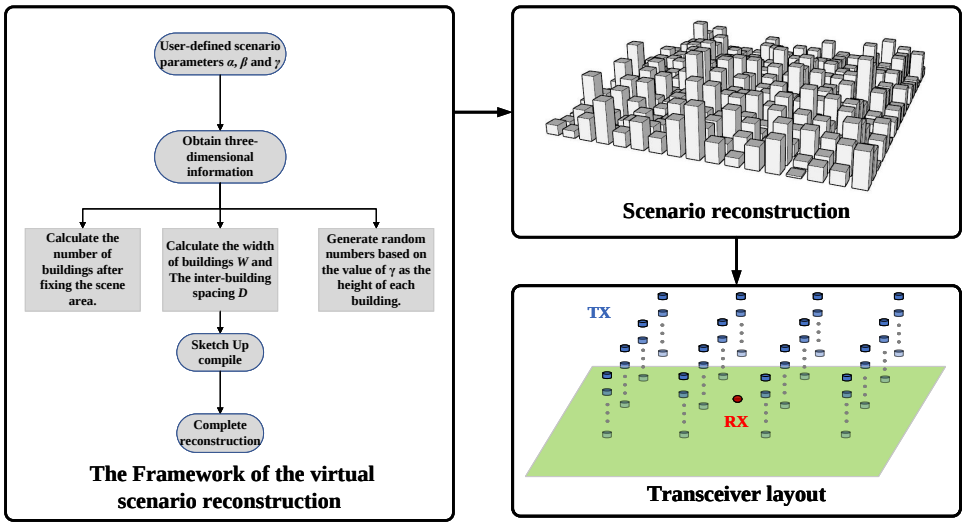

Figure 2. RT simulation setup.

reconstruction technique. This method draws on field measurements and statistical analyses to derive a statistical profile for scatter properties, particularly for buildings in urban scenarios. By acquiring statistical data from real environments, it simplifies the reconstruction process and reduces cost and complexity. Operators only need to specify the parameters, α, β and γ, mentioned in Section 2 to accomplish the 3D scenario reconstruction.

Taking, for example, a city block measuring 1,000 meters by 1,000 meters, the number of buildings per row is calculated as

$$b = floor\sqrt{\beta} \tag{11}$$

where the floor function is applied to guarantee that the quantity of terms in the calculation yields an integer number of buildings. The spacing between buildings D and the width of buildings W can be calculated easily according to the geometric relationship, expressed as

$$W = 1000\sqrt{\alpha/\beta} \tag{12}$$

$$D = \frac{1000}{\sqrt{\beta}} - W \tag{13}$$

Then, a series of random numbers are generated that matched the Rayleigh distribution with a mean value of γ, to the total number of buildings. These random numbers represent the heights of the buildings. With the 3D information of the urban environment, the building modeling can be accomplished using the Ruby Code Editor plugin in SketchUp.

The design of the RT simulation scheme plays a role in ensuring comprehensive and efficient data collection. For every scenario, the Rx is located in the center of the area, and the Txs are at different altitudes on several layers, each with hundreds of Tx uniformly distributed. At last, the building material is set to concrete. The scenario reconstruction and the layout of the transceivers are shown in Figure 2.

A software called Wireless Insite is used for RT simulation. The precision of the reconstructed digital map is 5 m. During the RT simulation, we set the order of reflections to be no more than two, and the order of the diffraction to be one. The channel parameters are computed through three steps, i.e., decomposition of ray source, tracking of rays, and superposition of filed strength [30]. The power received at each RX point is precisely determined and subsequently converted into amplitude as

Table 1. Four typical urban scenarios with characteristic parameters

Scenarios	α	β	γ
Suburban	0.1	750	8
Urban	0.3	500	15
Dense	0.5	300	20
Highrise	0.5	300	50

$$\alpha_o = 10^{\frac{A_o}{10}} \tag{14}$$

where A_o is the power of the oth path. The value of the PL can be expressed as

$$P = 10\log_{10}(\sum_{o=1}^{O} \alpha_o^2) \tag{15}$$

where O is the number of rays.

4. SIMULATIONS AND VALIDATIONS

4.1 Model training in limited scenarios

To validate the accuracy of the proposed PL prediction method, a large number of datasets are obtained through RT simulation, as mentioned in Section 3.2. For the LoS case, four typical urban scenarios are reconstructed for simulations according to the defined parameters in the ITU standard [28], as shown in Table 1. Three stochastic simulations are conducted for each typical scenario to account for the effects of different building heights; i.e., a total of 12 scenarios are considered. However, it is necessary to explore more scenarios for NLoS conditions. To cover more scene types, parameters are varied: α from 0.1 to 0.8 in 0.1 intervals, β from 100 to 800 in 100 intervals, and γ from 8 to 50 in two intervals. This approach includes 176 scenarios, producing a rich dataset. However, due to the delicate and efficient model, only eight of these scenarios are ultimately employed for network training. The Txs are deployed at six different heights, from 30 to 80 m in 10 m intervals, while the Rx is located in the center of the area at 25 m above the ground. In addition, we set the reflection and diffraction counts by RT simulation software to obtain LoS and NLoS datasets, respectively. The details of the specific simulation parameters are presented in Table 2.

Subsequently, the acquired RT simulation data is performed as a dataset for BPNN training. The learning rate is set to 0.0001, the momentum factor is set to 0.95, the number of training epochs is set to 2,000, and the hidden layer is set to a single layer consisting of 20 neurons. For the LoS case, there are 6,078 datasets, of which 4,862 are used for training and 1,216 for testing. Similarly, for the NLoS case, there are 49,230 datasets, of which 39,384 are used for training and 9,846 for testing. For the LoS case, there are 6,078 datasets, of which 4,862 are used for training and 1,216 for testing. Similarly, for the NLoS case, there are 49,230 datasets, of which 39,384 are used for training and 9,846 for testing. This division helps make the training of the network suitable for various scenarios.

In the LoS case, the effect of scenario parameters on PL is found to be minimal. Consequently, we focus on examining the dynamics between horizontal distance s, Tx height h and PL P, as depicted in Figure 3. It is observed that PL intensifies with the distance between the Tx and Rx. Importantly, the impact of horizontal distance on PL is more significant at lower altitudes compared to the effect of vertical separation. Figure 4A illustrates the analysis of the RT simulation data with the PL values predicted by the BPNN model, showing a high degree of correlation and highlighting the accuracy of the model. The deviation results are all less than 3 dB, as shown in Figure 4B. This further validates the reliability of the model and confirms the accuracy of

Table 2. Simulation parameters

Parameters	Value
Scenarios	4 for the LoS case, 8 for the NLoS case
Frequency (Bandwidth)	28 GHz (1 GHz)
Antenna type	Omnidirectional for both Rx and Tx
The height of Tx (interval)	30~80 m (10 m)
The height of Rx	25 m
Building material	Concrete
Maximum number of reflections	0 for LoS and 2 for NLoS
Maximum number of diffraction	0 for LoS and 1 for NLoS

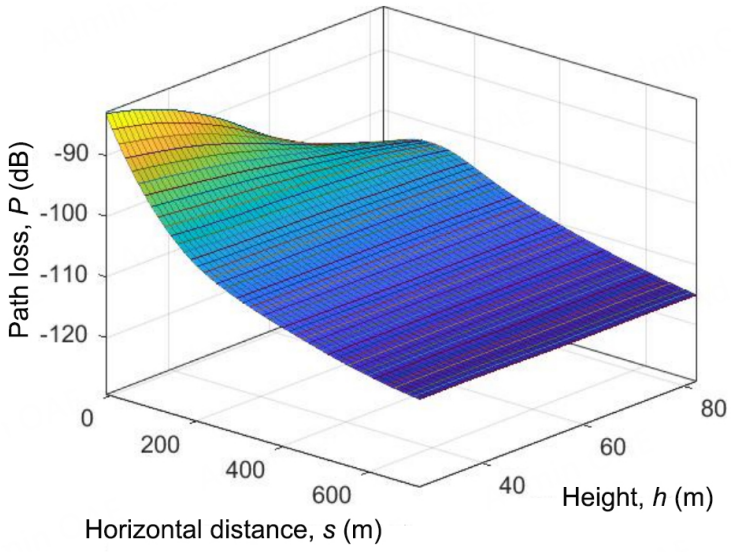

Figure 3. Simulated PL for the LoS case.

our prediction method. Additionally, the RMSE is determined to be 0.2493, following the calculation given in Equation (10).

In scenarios where the LoS path is obstructed, various environmental factors significantly influence PL. Figure 5-Figure 7 illustrate the relationship between the input factors and the PL in this case. Specifically, Figure 5 shows that an increase in Tx height leads to a reduction in PL. This phenomenon can be explained by a reduction in obstacle interference, since increasing the Tx height effectively lengthens the LoS path, thereby reducing signal attenuation caused by physical obstacles. Figure 6 shows that greater building coverage indicates a denser urban environment, where buildings are more likely to obstruct and weaken the signal, thereby increasing PL and negatively affecting signal quality. In addition, the presence of higher buildings increases the likelihood of signal blockage and reflection, further exacerbating PL, as evidenced in Figure 7.

Figure 8 demonstrates the performance of the NN. Obviously, the NN shows good prediction ability. About eighty percent of the deviation results are less than 5 dB and the RMSE is 8.27489.

4.2 Model validation in a new scenario

To further validate the effectiveness of our network, we introduce a new scenario setting with $\alpha = 0.4$, $\beta = 400$ and $\gamma = 18$ ensuring consistency with the network configurations used in previous experiments. Then, we

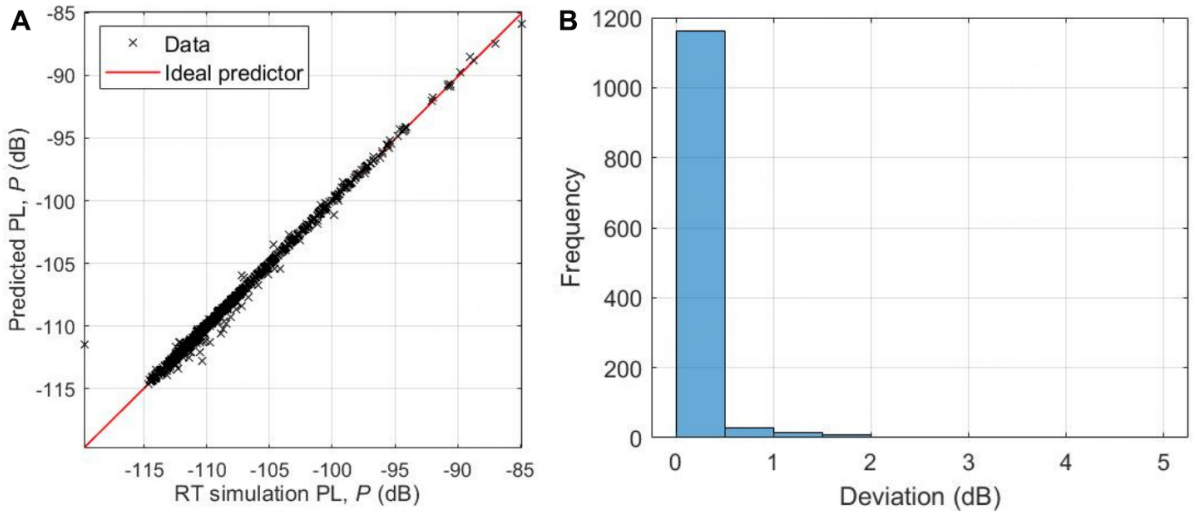

Figure 4. (A) Prediction accuracy and (B) Histogram of prediction error for the LoS case.

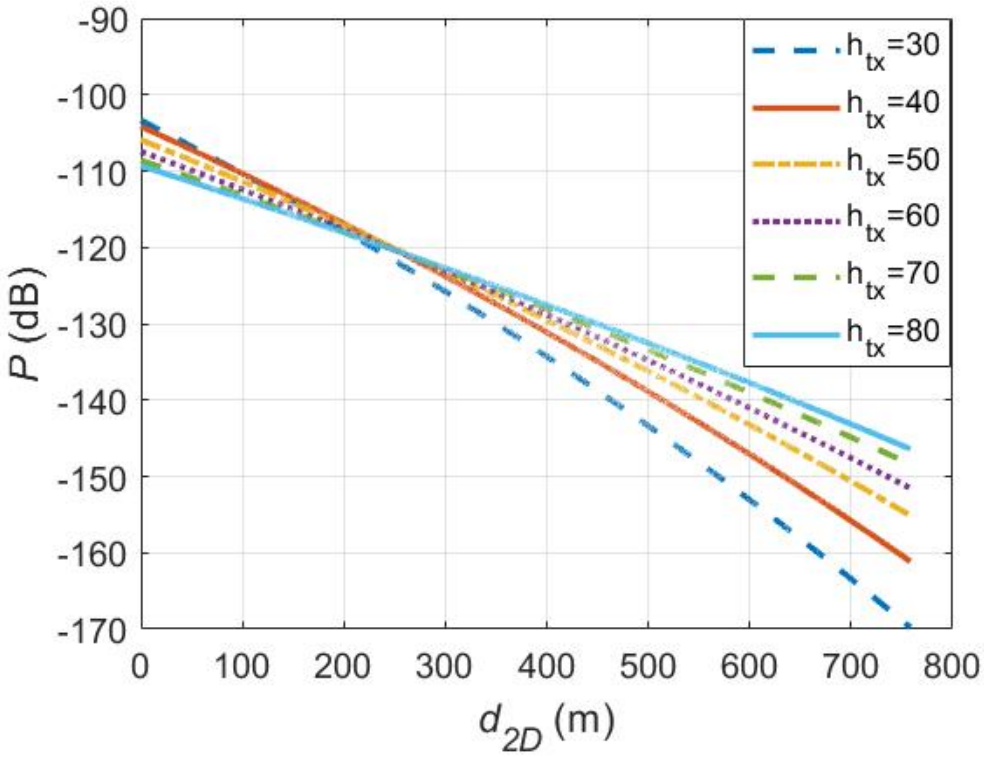

Figure 5. The impact of Tx height on PL for the NLoS case.

compare the PL values derived from the BPNN with RT simulations. The outcomes are depicted in Figure 9. The significant agreement between the BPNN predictions and the RT simulation data highlights the reliability and efficiency of our proposed method. Additionally, we also incorporate the concept of 3D distance between the Tx and the Rx, which is formulated as

$$d_{3D} = \sqrt{s^2 + (h - 25)^2} \tag{16}$$

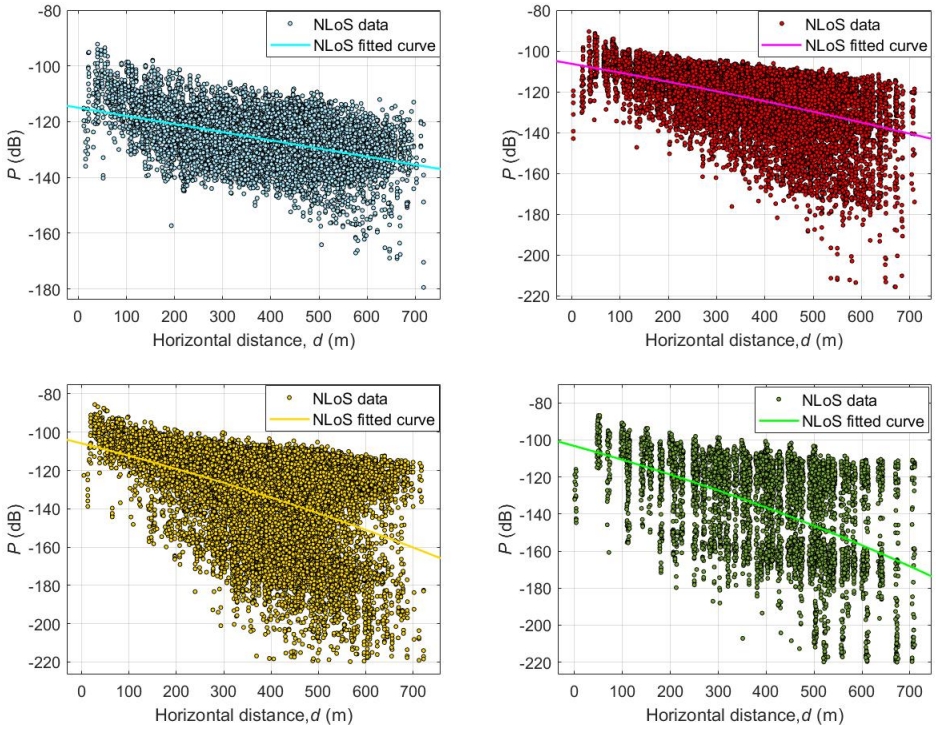

Figure 6. The impact of α on PL for the NLoS case (α=0.1, 0.3, 0.5 and 0.8, respectively).

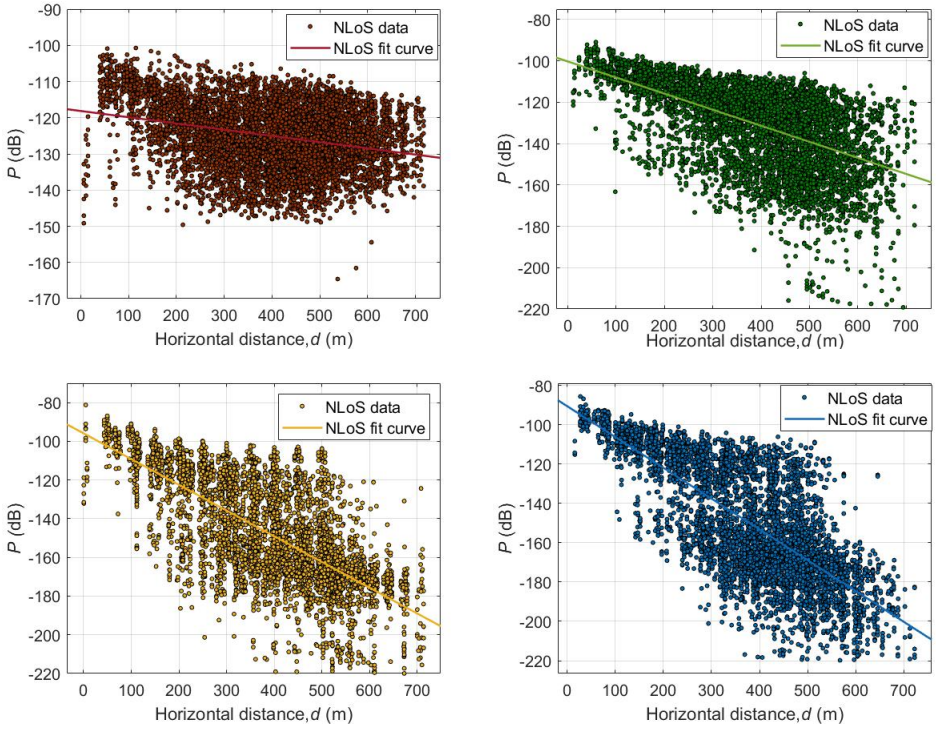

Figure 7. The impact of γ on PL for the NLoS case (γ=10, 30, 40 and 50, respectively).

For comparison, traditional prediction methods such as the 3GPP model were also simulated and the results are shown in Figure 10 and Figure 11. It should be emphasized that the 3GPP PL results are calculated us-

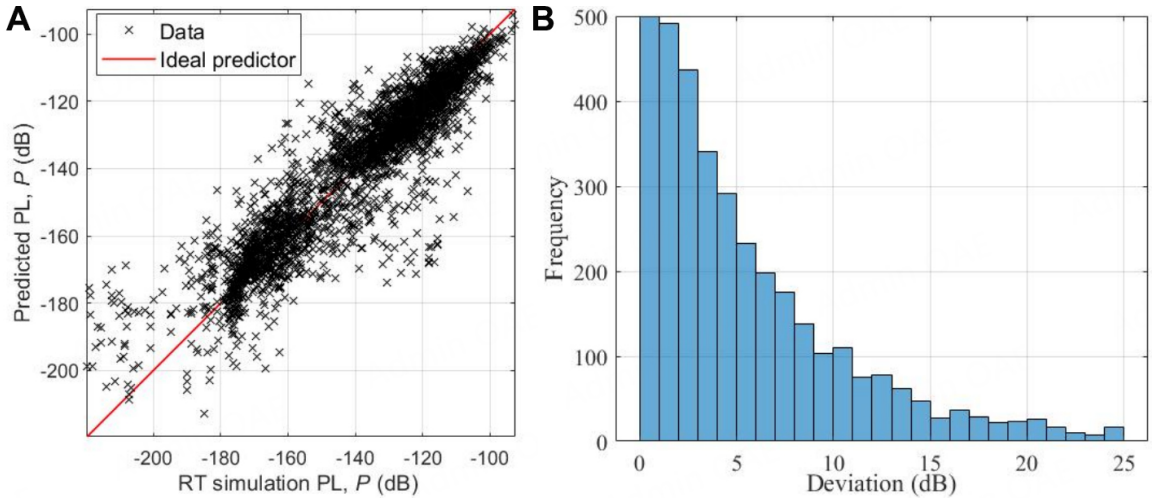

Figure 8. (A) PL prediction accuracy and (B) Histogram of prediction error for the NLoS case.

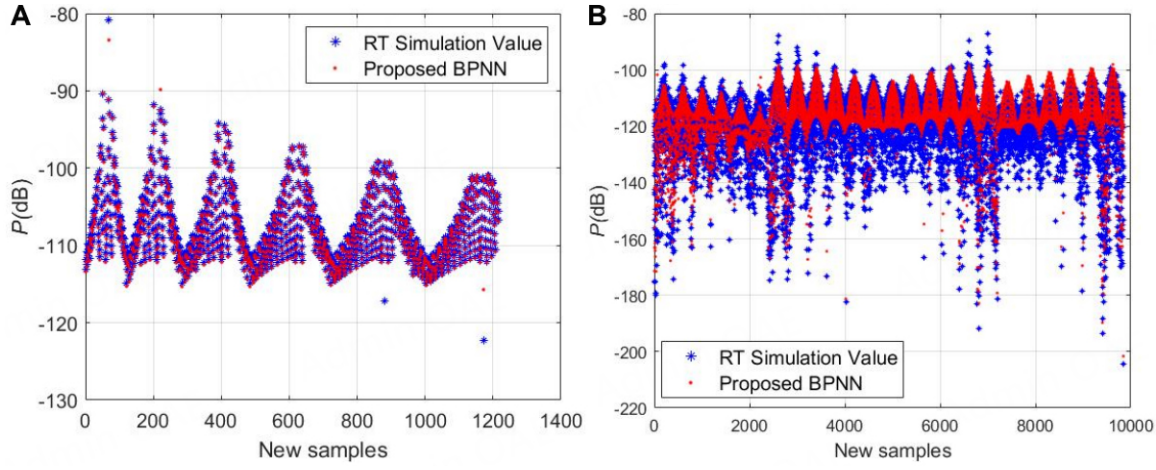

Figure 9. Predicted PL for (A) LoS and (B) NLoS case in the new scenario (α =0.4, β = 400 and γ = 18).

ing the LoS/NLoS path formulae for RMa scenarios[20]. This comparative analysis clearly demonstrates the enhanced performance of our proposed prediction method compared to traditional methods. Our model is tailored to the specific scenario data and utilizes ML techniques, which has a significant correlation with the simulation results. On the contrary, the 3GPP model, which is usually applied to Rx at lower heights (0-10 meters), demonstrates a less accurate predictive capability in specific scenarios. Looking ahead, this comparison underscores the potential of ML-based methods to address limitations in traditional models, particularly in scenarios with higher Rx heights or more complex scenarios. Future research could build on the three scenario parameters in this paper by further exploring additional environmental feature parameters (e.g., terrain relief), integrating them into the ML model, and validating their performance in a wider range of scenarios. This approach may bring more powerful prediction tools and facilitate advances in wireless network planning and optimization.

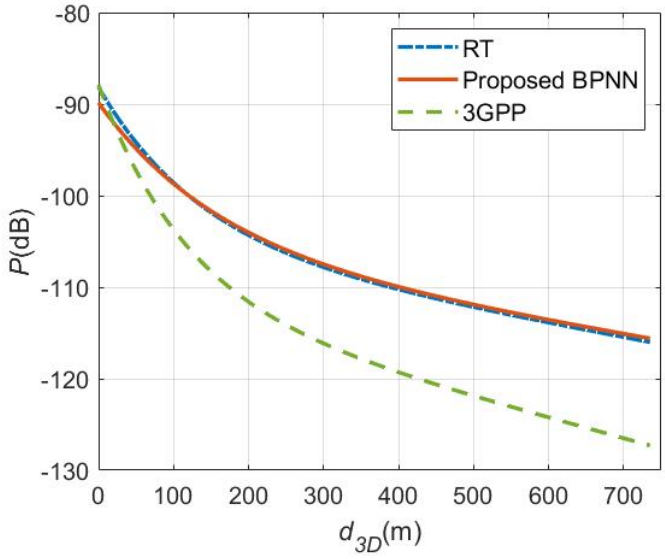

Figure 10. Predicted PL of different methods in the LoS case (α = 0.4, β = 400, and γ =18).

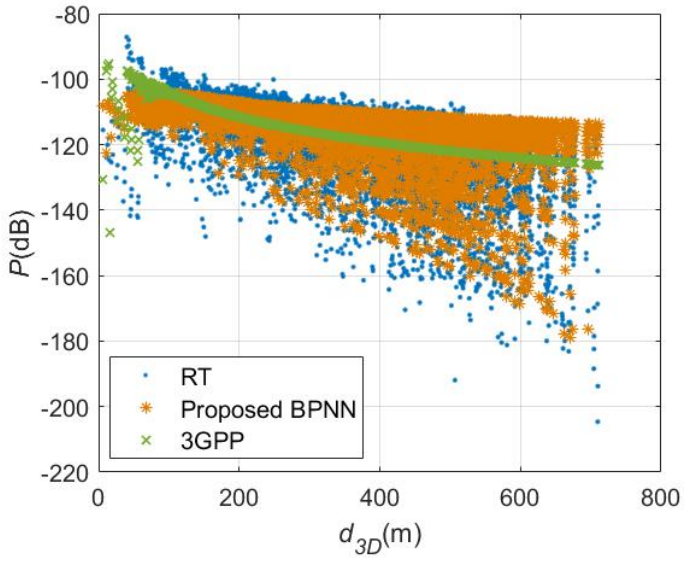

Figure 11. Predicted PL of different methods in the NLoS case (α = 0.4, β = 400, and γ = 18).

5. CONCLUSIONS

This paper has proposed a cross-scenario PL prediction model based on BPNN for A2G communications. The model has demonstrated the ability to accurately forecast the power for both LoS and NLoS paths trained with extensive RT simulation data across a variety of urban environments. A correlation has been established between the PL and scenario parameters, horizontal distance, and altitude. The performance of trained BPNN has been evaluated against a new scenario dataset derived from RT simulations and 3GPP standard model, confirming the superiority of the proposed method over traditional PL prediction approaches. In the future, we will develop an mmWave A2G channel sounder for further validating the proposed method via field measurements.

DECLARATIONS

Authors' contributions

Made substantial contributions to conception and design of the study and performed data analysis and interpretation: Zhang G, Lei T, Huo X

Contributed to approach validation, software simulation, and writing-original draft preparation: Zhang G, Li Y, Geng M, Yang Y

Contributed to the investigation, supervision, and writing-review and preparation: Yang H, Chen X

Availability of data and materials

Not applicable.

Financial support and sponsorship

None.

Conflicts of interest

Huo X is affiliated with Qingdao Metro Group Co., Ltd, while the other authors have declared that they have no conflicts of interest.

Ethical approval and consent to participate

Not applicable.

Consent for publication

Not applicable.

REFERENCES

1. Na Z, Liu Y, Shi J, Liu C, Gao Z. UAV-supported clustered NOMA for 6G-enabled internet of things: trajectory planning and resource allocation. *IEEE Int Things J* 2021;8:15041-8. DOI
2. Hua B, Ni H, Zhu Q, et al. Channel modeling for UAV-to-ground communications with posture variation and fuselage scattering effect. *IEEE Trans Commun* 2023;71:3103-16. DOI
3. Mao K, Zhu Q, Qiu Y, et al. A UAV-aided real-time channel sounder for highly dynamic nonstationary A2G scenarios. *IEEE Trans Instrum Meas* 2023;72:6504515. DOI
4. Xiong B, Zhang Z, Jiang H, Zhang J, Wu L, Dang J. A 3D non-stationary MIMO channel model for reconfigurable intelligent surface auxiliary UAV-to-ground mmWave communications. *IEEE Trans Wireless Commun* 2022;21:5658-72. DOI
5. Pi Z, Khan F. An introduction to millimeter-wave mobile broadband systems. *IEEE Commun Mag* 2011;49:101-7. DOI
6. Zhao X, Du F, Geng S, et al. Playback of 5G and beyond measured MIMO channels by an ANN-based modeling and simulation framework. *IEEE J Sel Areas Commun* 2020;38:1945-54. DOI
7. Alkhateeb A, El Ayach O, Leus G, Heath RW. Channel estimation and hybrid precoding for millimeter wave cellular systems. *IEEE J Sel Top Signal Process* 2014;8:831-46. DOI
8. Liu X, Wang J, Zhao N, et al. Placement and power allocation for NOMA-UAV networks. *IEEE Wireless Commun Lett* 2019;8:965-8. DOI
9. Phillips C, Sicker D, Grunwald D. A survey of wireless path loss prediction and coverage mapping methods. *IEEE Commun Surv Tutor* 2013;15:255-70. DOI
10. Ayadi M, Ben Zineb A, Tabbane S. A UHF path loss model using learning machine for heterogeneous networks. *IEEE Trans Antennas Propag* 2017;65:3675-83. DOI
11. Mao K, Zhu Q, Duan F, et al. A2G channel measurement and characterization via TNN for UAV multi-scenario communications. In: GLOBECOM 2022 - 2022 IEEE global communications conference; 2022. pp. 4461-6. DOI
12. Sarkar TK, Ji Z, Kim K, Medouri A, Salazar-Palma M. A survey of various propagation models for mobile communication. *IEEE Antennas Propag Mag* 2003;45:51-82. DOI
13. Mao K, Zhu Q, Wang CX, Ye X, Gomez-Ponce J, et al. A survey on channel sounding technologies and measurements for UAV-assisted communications. *IEEE Trans Instrum Meas* 2024;73:8004624. DOI

14. He D, Ai B, Guan K, Wang L, Zhong Z, Kurner T. The design and applications of high-performance ray-tracing simulation platform for 5G and beyond wireless communications: A tutorial. *IEEE Commun Surv Tutor* 2019;21:10-27. DOI
15. Zhu Q, Mao K, Song M, et al. Map-based channel modeling and generation for U2V mmWave communication. *IEEE Trans Veh Technol* 2022;71:8004-15. DOI
16. Hossain F, Geok TK, Rahman TA, et al. A smart 3D RT method: indoor radio wave propagation modelling at 28 GHz. *Symmetry* 2019;11:510. DOI
17. Cui Z, Guan K, Oestges C, Briso-Rodríguez C, Ai B, Zhong Z. Cluster-based characterization and modeling for UAV air-to-ground time-varying channels. *IEEE Trans Veh Technol* 2022;71:6872-83. DOI
18. Lyu Y, Wang W, Chen P. Fixed-wing UAV based air-to-ground channel measurement and modeling at 2.7GHz in rural environment. *IEEE Trans Antennas Propag* 2024;1. DOI
19. Lyu Y, Wang W, Sun Y, Rashdan I. Measurement-based fading characteristics analysis and modeling of UAV to vehicles channel. *Veh Commun* 2024;45:100707. DOI
20. 3GPP. Evolved Universal Terrestrial Radio Access (E-UTRA); Radio Resource Control (RRC); Protocol specification. 3rd Generation Partnership Project (3GPP); 2017. 36.331. Version 14.2.2.
21. Döttling M, Mohr W, Osseiran A. Radio technologies and concepts for IMT-advanced. John Wiley & Sons; 2010. Available from: http://dx.doi.org/10.1109/pesa.2017.8277746 [Last accessed on 29 Sep 2024]
22. Cui Z, Briso-Rodríguez C, Guan K, Zhong Z, Quitin F. Multi-frequency air-to-ground channel measurements and analysis for UAV communication systems. *IEEE Access* 2020;8:110565-74. DOI
23. Rappaport TS. Wireless Communications: Principles and Practice. USA: Prentice Hall PTR; 2001. Available from: https://telkom2013.wordpress.com/wp-content/uploads/2014/02/wireless-comm-princip-n-practice-theodoresrappaport.pdf [Last accessed on 29 Sep 2024]
24. Cai X, Rodríguez-Piñeiro J, Yin X, et al. An empirical air-to-ground channel model based on passive measurements in LTE. *IEEE Trans Veh Technol* 2019;68:1140-54. DOI
25. Yang G, Zhang Y, He Z, Wen J, Ji Z, Li Y. Machine-learning-based prediction methods for path loss and delay spread in air-to-ground millimetre-wave channels. *IET Microw Antennas Propag* 2019;13:1113-21. DOI
26. Li H, Chen X, Mao K, et al. Air-to-ground path loss prediction using ray tracing and measurement data jointly driven DNN. *Comput Commun* 2022;196:268-76. DOI
27. Huang Y, Cui H, Hou Y, et al. Space-based electromagnetic spectrum sensing and situation awareness. *Space Sci Technol* 2024;4:0109. DOI
28. Union IT. Propagation data and prediction methods for the planning of short-range outdoor radiocommunication systems and radio local area networks in the frequency range 300 MHz to 100 GHz; 2003. pp. 1411-2. Available from: https://www.itu.int/rec/R-REC-P.1411-12-202308-I/en [Last accessed on 29 Sep 2024]
29. Isabona J, Srivastava VM. Hybrid neural network approach for predicting signal propagation loss in urban microcells. In: 2016 IEEE region 10 humanitarian technology conference (R10-HTC); 2016. pp. 1-5. DOI
30. Wang J, Zhu Q, Lin Z, et al. Sparse bayesian learning-based hierarchical construction for 3D radio environment maps incorporating channel shadowing. *IEEE Trans Wirel Commun* 2024;1. DOI